International Journal of Engineering Trends and Technology
ISSN: 2231–5381 / https://doi.org/10.14445/22315381/IJETT-V74I2P108

Volume 74 Issue 2, 113-124, February 2026

Original Article

An Improved Hybrid LED Driver

Dzhunusbekov Erlan[1], Orazbayev Sagi[2]

[1]*Laboratory of Electronics, Kazakh-British Technical University, Kazakhstan.*
[2]*Engineering Laboratory of the Al-Farabi National University, Kazakhstan.*

[1]*Corresponding Author : e.dzhunusbekov@kbtu.kz*

Received: 03 September 2025 Revised: 02 January 2026 Accepted: 20 January 2026 Published: 14 February 2026

Abstract *- The continuous improvement of solid-state lighting technologies demands efficient and reliable LED drivers capable of minimizing switching losses while maintaining high power quality. Even a slight improvement in efficiency can have a significant economic impact, given the widespread adoption of LED lighting. This paper presents an experimental investigation of an improved hybrid LED driver that combines dynamic LED string reconfiguration with a low-power auxiliary switching stage to enhance efficiency. The proposed architecture employs protective diodes connected in series with MOSFETs, which effectively reduce switching stress without introducing significant conduction losses. A 200 W laboratory prototype with five LED strings was developed and tested under input voltages of 160-270 Vac at 50 Hz. Simulation and experimental results demonstrate good agreement, confirming the theoretical predictions. The prototype achieved a peak efficiency of 98.6% at 230 VAC, with a power factor of 0.98 and a total harmonic distortion of 11%. The experimental study confirms the practical feasibility and relative simplicity of the proposed improved hybrid driver. The switching transients and voltage stresses on transistors and diodes were significantly reduced. Low switching losses and the limited conduction losses of the protection diodes make it feasible to achieve future monolithic integration, combining not only the power transistors and control circuitry but also the protection diodes within a single chip.*

Keywords *- Capacitorless LED driver, Direct AC LED module, Hybrid LED driver, High voltage LED driver, LED street lighting.*

1. Introduction

The continuous advancement of solid-state lighting technologies, particularly Light-Emitting Diodes (LEDs), has spurred extensive research into efficient and reliable LED driver circuits. A major objective of these studies is to enhance the performance, cost-effectiveness, and reliability of LED drivers, which remain the weakest link in modern lighting systems due to their shorter lifetimes, higher failure rates, and greater cost contribution compared to high-tech LEDs [1-8].

A growing trend in LED driver design is the integration of control and power stages into a single chip, with the aim of reducing cost, board space, and the number of potential failure points.

One promising approach is the development of direct AC LED drivers [9-16], which eliminate the complex Switch-Mode Power Supply (SMPS) in favor of a relatively simple low-frequency logic circuit. In this approach, the LED load is segmented, and the segments are dynamically lined up by the logic control synchronously with the AC line frequency to match the alternating mains voltage. To compensate for the mismatch between the voltage of LED segments and the instantaneous line voltage, a linear current regulator is employed. This architecture reduces system complexity and minimizes component count. It can operate without electrolytic–capacitors, thereby improving reliability [7, 8]. Recent advancements [15] include the integration of control logic with linear current regulators, enabling compact designs and cost reductions compared to conventional SMPS. Despite these advantages, AC direct LED drivers face challenges due to their reliance on linear current regulation, which leads to significant conduction losses, thermal issues, and limited scalability to higher power levels.

In an effort to overcome these limitations, the hybrid LED Driver architecture has been proposed and explored in recent literature [17-19]. This design retains the concept of a dynamically reconfigurable segmented LED load, similar to that of direct AC LED modules, aligning LED strings with the alternating mains waveform. The idea is to incorporate a small, efficient auxiliary power stage - typically consisting of a low-power inductor and MOSFETs - controlled by an optimized switching algorithm - to compensate for the voltage difference between the input mains voltage and the LEDs. Since only a fraction of the total power is processed by this auxiliary stage, overall system losses would remain low. However, because the slow LED strings are driven directly by

transistors operating in high-frequency switch-mode, both the LEDs and power MOSFETs are subjected to hard switching, which compromises reliability, efficiency, and EMI performance at higher power levels. Therefore, these designs are still limited to low-power and low-voltage applications. In [18], the developed prototype achieved an efficiency of 95.1% at a 110 Vac mains input and a 20W output, with the LED load divided into seven segments.

To meet the strong demand for high-power, high-voltage, and high-efficiency LED drivers, simply dividing the LED load into smaller strings to reduce the amplitude of the pulsed voltages across semiconductor devices does not resolve the problem, as the hard-switching issue remains.

In this work, an improved high-power, high-efficiency hybrid LED driver is proposed, capable of operating with input voltages up to 275Vac. The proposed driver utilizes an LED load divided into only five strings, along with four governing power transistors. Such a driver became realizable because the hard switching of the power semiconductors is alleviated by the introduction of four protection diodes. The diodes are connected in series with the transistors to limit conduction losses and thereby achieve higher efficiency compared to a conventional boost LED driver. Computer-based simulations and an experimental study of a 200W laboratory prototype are provided. The feasibility and major performance claims of the hybrid LED driver were experimentally confirmed.

This paper is structured as follows: Section 2 proposes the improved hybrid LED driver and revisits the operating principle of the proposed hybrid driver; Section 3 outlines the experimental setup; Section 4 reports the experimental findings and discusses the findings along with their implications and potential areas for further research; and Section 5 concludes the study.

2. The Proposed Hybrid LED Driver

The proposed hybrid LED driver is shown in Figure 1. Resembling conventional hybrid LED drivers, the load consists of multiple LED strings, LED_0-LED_4, connected in a dynamically reconfigurable series arrangement. The four strings, LED_1-LED_4, are controlled by four power transistors Q_1-Q_4, enabling a four-stage driver configuration. As the instantaneous input voltage increases within the AC half-cycle, additional LED strings are sequentially connected in series; as the voltage decreases, they are disconnected. This dynamic configuration substantially reduces the pulse amplitude on the power components in a typical hybrid LED driver, limiting it to the voltage drop across a single LED string.

The distinctive features of the proposed driver, shown in Figure 1, are as follows. The driver includes protective diodes D_1-D_4 to prevent reverse current flow through the LED strings, which is critical for reliable operation in high-power and high-voltage applications. As a result, switching losses in power semiconductors are significantly reduced, enabling the development of LED drivers with power ratings of 200W and beyond. The novelty of the circuit lies in connecting the protective diodes D_1-D_3 in series with their corresponding power transistors Q_1-Q_3. In this configuration, only two diodes participate in PWM operation, functioning complementarily so that only one conducts at a time. As a result, the total conduction losses of all diodes are limited to those of a single conducting diode at any given time, enabling the development of a high-efficiency driver. This diode configuration allows the driver to incorporate additional LED strings or break the LED load into smaller segments without increasing the overall diode conduction losses.

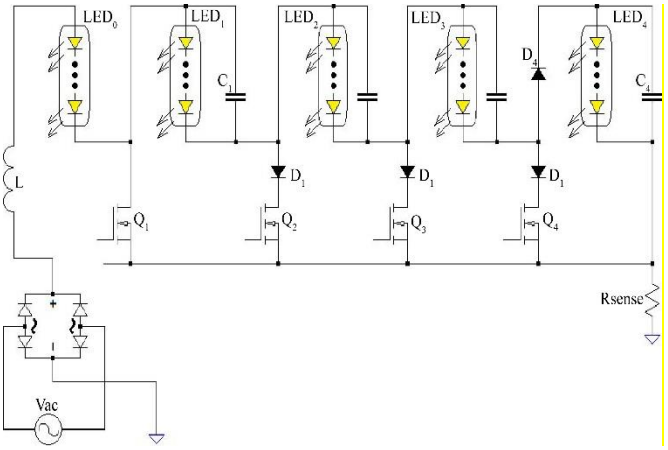

Fig. 1 The proposed hybrid LED driver

The protective diode D_4 is connected on the high side of the LED_4 string, which helps to reduce EMI noise, stabilize the control process, and ensure reliable switching transitions at high input voltage values.

The LED_0 string is connected in series with the main inductor and is not controlled by any switching device. The inclusion of LED_0 serves several important functions. First, it reduces both the impulse and absolute voltage stresses on the power transistors and protective diodes, as part of the input voltage is dropped across this string without requiring the addition of another switching stage. Second, the hybrid driver produces pulsed switching only when the instantaneous input voltage satisfies $|Vin| > V_{LED0}$. Consequently, the circuit enters a skip-mode at low input voltages, thereby avoiding low-efficiency regions and improving the overall energy performance. Finally, the driver was developed with the LED load segmented into five LED strings, achieved with only four active transistors and four operating stages.

For D_1 and D_2, Schottky diodes are employed due to the low absolute voltage stress on the diodes located near the input. This choice reduces both conduction and switching losses compared to conventional fast-recovery diodes.

Furthermore, the voltage stress on the high-current transistors Q_3 and Q_4, situated closer to the load, is relatively low, enabling the use of low-voltage MOSFETs with low on-state resistance $R_{DS(on)}$, which further improves overall driver efficiency.

The protective diodes D_1-D_4 make it possible to place smoothing capacitors C_1-C_4 across the LED strings to improve operating conditions of the LEDs or to reduce light flicker.

In the proposed driver shown in Figure 1, increasing the number of LED strings (i.e., operating stages) beyond five yields no meaningful reduction in switching losses relative to the conduction losses of the bridge diodes, while unnecessarily increasing circuit complexity.

2.1. Theoretical Analysis

The working principle is as follows. For a given input voltage *Vin*, if the sum of LED voltages satisfies the condition $V_{LED0}+V_{LED1}+...+V_{LED(K-1)}<Vin<V_{LED0}+V_{LED1}+ \ ... \ ...+V_{LED(K)}$, then Stage(K) of PWM regulation is activated: transistors Q_1 to Q_{K-1} are in non-conducting state, transistors Q_{K+1} to Q_4 are in ON state, but only Q_K actively regulates the input current, operating in switch mode.

As an example, for a driver operating in Continuous Conduction Mode (CCM), consider the condition where the input voltage satisfies Equation 1:

$$V_{LED0} + V_{LED1} + V_{LED2} < Vin < \\ < V_{LED0} + V_{LED1} + V_{LED2} + V_{LED3} \quad (1)$$

In this case, the driver operates in Stage(3), and the control circuit regulates the inductor current I_L by pulse-width modulation (PWM) of the switch Q_3. During this stage, as shown in Figure 2(a), when Q_3 is conducting, the LED strings LED_0-LED_2 and the inductor L are connected in series with the input source *Vin*. The inductor current I_L rises from the lower current threshold to the upper threshold, since the condition in Equation 1 is satisfied. At this time, only one protective diode, D_2, conducts the inductor current, while diode D_3 is reverse-biased by the stored charge voltage of the LED_3 string, and the voltage across diode D_4 equals V_{LED3} + V_{LED4}.

When the inductor current reaches the upper threshold, transistor Q_3 turns off, and the inductor L, together with the LED strings LED0-LED3, is connected in series with the source *Vin*, as illustrated in Figure 2(b). The current I_L then decreases until it reaches the lower reference threshold. During this period, only diode D_3 conducts the inductor current, while diode D_4 remains reverse-biased by the residual stored charge voltage of the LED_4 string. During Stage(3), as the switch Q_3 operates in PWM mode, all semiconductor devices experience equal pulse voltage amplitudes equal to V_{LED3}, although their absolute voltage levels differ. Thus, it can be generalized that at any Stage(K), all semiconductors in Figure 2 are subjected to pulsed voltages corresponding to the forward voltage drop $V_{LED(K)}$ of the active LED_K string. The closer the transistor Q_K is to the input source *Vin*, the higher the absolute voltage value it experiences. The maximum voltage stress is on transistor Q_1, and equals $V_{Q1} = Vin - V_{LED0}$. Conversely, the farther the protective diode D_K is from the source, the higher the voltage across it. The maximum reverse voltage on the protective diode is $V_{D4} = V_{LED1}+...+V_{LED4}$.

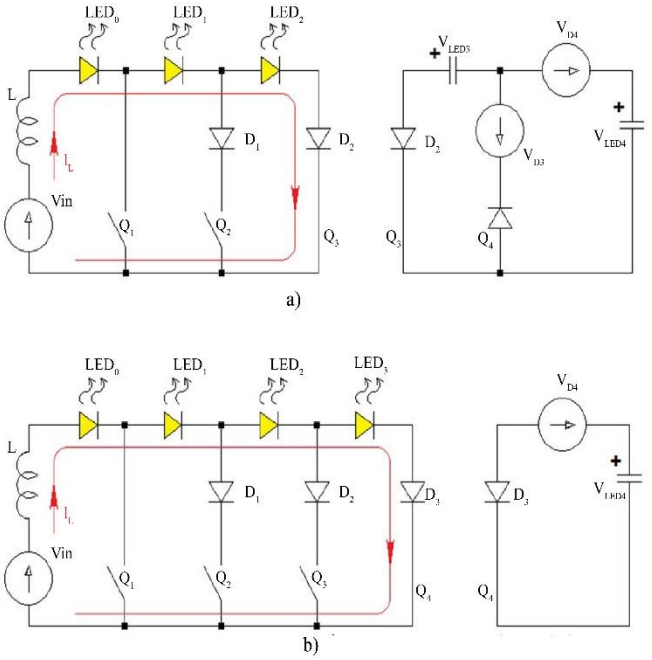

Fig. 2 The equivalent circuit of the proposed driver at the working Stage(K): (a) key Q3 conducts, and (b) key Q3 does not conduct.

When the input voltage increases and reaches $V_{LED0}+V_{LED1}+...+V_{LED3}$, the hybrid driver transitions to Stage(4). When the input voltage decreases to $V_{LED0}+V_{LED1}+V_{LED2}$, the driver switches to operation Stage(2). The theoretical analysis shows that at any Stage(K), only the diode pair D_{K-1} and D_K alternately conducts, while all other diodes remain inactive and do not carry current. At any given time, only one protective diode conducts current, which minimizes conduction losses. In practice, the method of stage transition based on the input voltage level was not applied because the input voltage contains network noise and interference. Such disturbances could cause false transitions between stages and increase the harmonic distortion of the input current. Therefore, in both the experimental prototype and computer simulations, a current-based control strategy was used. This approach acts as a natural filter — transitions occur only when physically meaningful current thresholds in the inductor are reached, which makes the circuit more stable and robust.

2.2. Computer Modeling and Analysis

Computer simulations were performed to compare the calculated data with experimental results. The developed simplified computer model is shown in Figure 3.

To coincide with the experimental sample, the voltage drops of LED strings are chosen to be - V_{LED0}=80V, V_{LED1}=80V, V_{LED2}=90V, V_{LED3}=90V, V_{LED4}=60V, as in the experimental sample. This results in a total output LED voltage of 400V. With V_{LED0}=80V, this does not have much influence on the Power Factor (PF) and THD, as confirmed by experiments.

The proposed driver can work without the electrolytic capacitors across the LED strings. But in this simulation scenario and in experiments, an implementation with electrolytic capacitors is considered. With electrolytic capacitors, the LEDs receive a continuous current supply, making power flow easier to analyze in simulations and to measure in experiments for efficiency estimation.

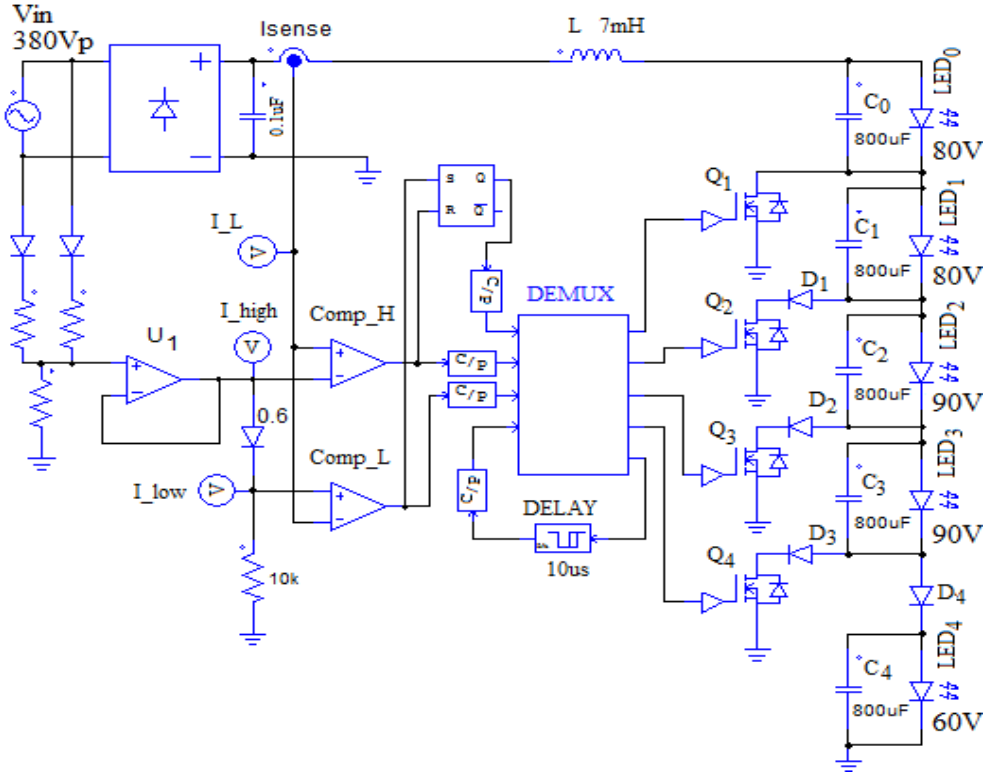

Fig. 3 Computer simulation model of the proposed hybrid LED driver

A hysteresis current control method was implemented using a current sensor and comparators Comp_L and Comp_H with corresponding references *I_low* and *I_high*. The DEMUX block in Figure 3 manages the transition between stages, Stage(K)↔Stage(K+1), if some conditions are met. At an active Stage(K), the DEMUX directs the modulated pulse signal from the flip-flop trigger to an appropriate gate of the currently active transistor Q_K, while holding gates of transistors Q_1 through Q_{K-1} at zero and keeping gates of transistors Q_{K+1} through Q_4 at a high level. Therefore, in Stage(K), transistor Q_K operates in PWM mode: if the inductor current reaches a high threshold, Q_K changes to the OFF-state; if the inductor current reaches a low threshold, Q_K changes to the ON-state. Stage transitions (K-1) ↔(K) are triggered by the comparator thresholds *I_low* and *I_high* using a hit/delay logic rule. This approach prevents chatter near zero-crossing points and suppresses false or mistimed transitions caused by noise in the mains voltage sensing. The transition process inside the DEMUX block follows this algorithm. If the inductor current reaches *I_high* and does not drop within the timeout period (DELAY), the system transitions from Stage(K) to Stage(K+1). That means that the LED_K string is added constantly in series with the inductor L, while the LED_{K+1} string becomes engaged in PWM regulation. Conversely, if the inductor current reaches *I_low* and does not rise within the timeout period (DELAY), the transition from Stage(K) to Stage(K−1) occurs. That means the LED_{K-1} string is engaged in PWM operation instead of LED_K. The algorithm also remains functional in scenarios involving a double threshold hit, where the inductor current reaches the same comparator threshold a second time after failing to cross the opposite threshold. In simulation, the input voltage is set to *Vin*=270Vrms, input power 200W. For better visualization, the inductor L is selected as 7mH to reduce the switching frequency and make the pulse switching traceable throughout the input phase cycle.

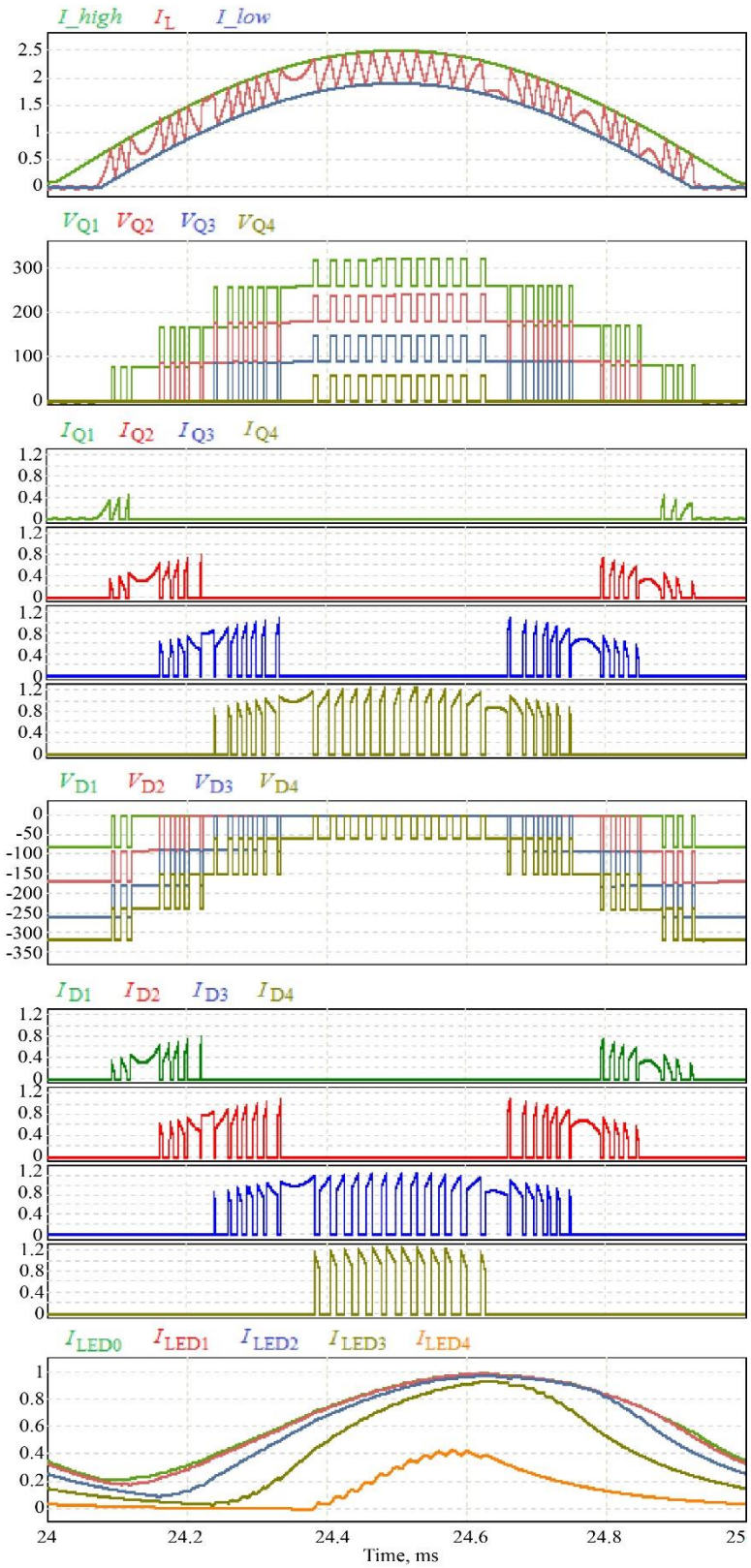

Fig. 4 Simulation waveforms of the proposed LED driver. *I_high, I_low,* I_L - comparators high/low values and inductor L current expressed in amperes (A); V_{Q1}, V_{Q2}, V_{Q3}, V_{Q4}- drain voltages on Q_1-Q_4 transistors expressed in voltages (V); I_{Q1}, I_{Q2}, I_{Q3}, I_{Q4} - currents of Q_1-Q_4 transistors expressed in amperes (A); V_{D1}, V_{D2}, V_{D3}, V_{D4} - reverse voltages on diodes D_1-D_4 expressed in voltages (V); I_{D1}, I_{D2}, I_{D3}, I_{D4} - currents of diodes D_1-D_4 expressed in amperes (A); I_{LED1}, I_{LED2}, I_{LED3}, I_{LED4} - currents of corresponding LED strings expressed in amperes (A).

Figure 4 presents the steady-state waveforms obtained from the computer simulation for a single half-cycle of the input voltage. The design demonstrates reduced voltage swings on inductor L, power transistors Q_1-Q_4, and across rectifier diodes D_1-D_4. The voltage swings are not more than 90V and equal to the LED string voltage $V_{LED(K)}$ in each Stage(K) that is currently active. The peak voltage across the diodes is: $V_{D1}=V_{LED1}=80V$, $V_{D2}=V_{LED1}+V_{LED2}=170V$, $V_{D3}=V_{LED1}+..+V_{LED3}=260V$, $V_{D4}=V_{LED1}+..+V_{LED4}=320V$. The average currents through transistors Q_K increase with index K. But while the index K increases, the total drain voltages $V_{Q(K)}$ are reduced from transistor Q_1 to Q_4: $V_{Q1}=V_{LED4}+..+V_{LED1}=320V$, $V_{Q2}=V_{LED4}+..+V_{LED2}=240V$, $V_{Q3}=V_{LED4}+V_{LED3}=150V$, $V_{Q4}=V_{LED4}=60V$. As shown in Figure 4, when the inductor current reaches the *I_high* threshold twice consecutively, an additional LED string is connected in series, leading to a current decrease. Conversely, when the inductor current reaches the *I_low* threshold twice in succession, one of the LED strings is short-circuited, causing the current to increase. These stage transitions take finite time and distort the power factor, because during these times the average inductor current deviates from the required sinusoidal average current. On the other hand, power factor can be improved by reducing the inductor value, thus decreasing the transition time. Or by decreasing hysteresis, this will bring the inductor current closer to a required average value.

Since the simulation was provided for 270Vac input, all stages are engaged during the mains input voltage cycle, see Figure 4, because input peak voltage *Vin*=381V satisfies: $340V=V_{LED0}+...+V_{LED3}<Vin<V_{LED0}+...+V_{LED4}=400V$. At input 230Vac, only the first three stages will be activated during the input cycle because the input peak voltage *Vin*=324V satisfies: $250V=V_{LED0}+...+V_{LED2}<Vin<V_{LED0}+...+V_{LED3}=340V$. At input voltage 160Vac, only the first two stages are activated because peak *Vin*=226V satisfies: $80V=V_{LED0}+V_{LED1}<Vin<V_{LED0}+...+V_{LED2}=240V$.

Based on the simulation results, the optimum values of voltage drops on the LED strings were chosen. With $V_{LED1}=80V$ and $V_{LED2}=90V$, Schottky diodes with rated voltages of 100V and 200V can be implemented for D_1 and D_2, respectively. With $V_{LED0}=80V$, the diode D_4 can be selected with a maximum rated voltage of 400V with a good margin. With $V_{LED3}=90V$, during the input phase cycle at *Vin*=230Vac, only the first four LED strings and three diodes D_1-D_3 are involved, which limits the conduction losses of the diodes; therefore, the driver is capable of reaching the highest efficiency at nominal input voltage. The simulation confirmed the feasibility of the proposed driver and the control logic. The control principles developed during the modeling stage were subsequently implemented in the laboratory prototype.

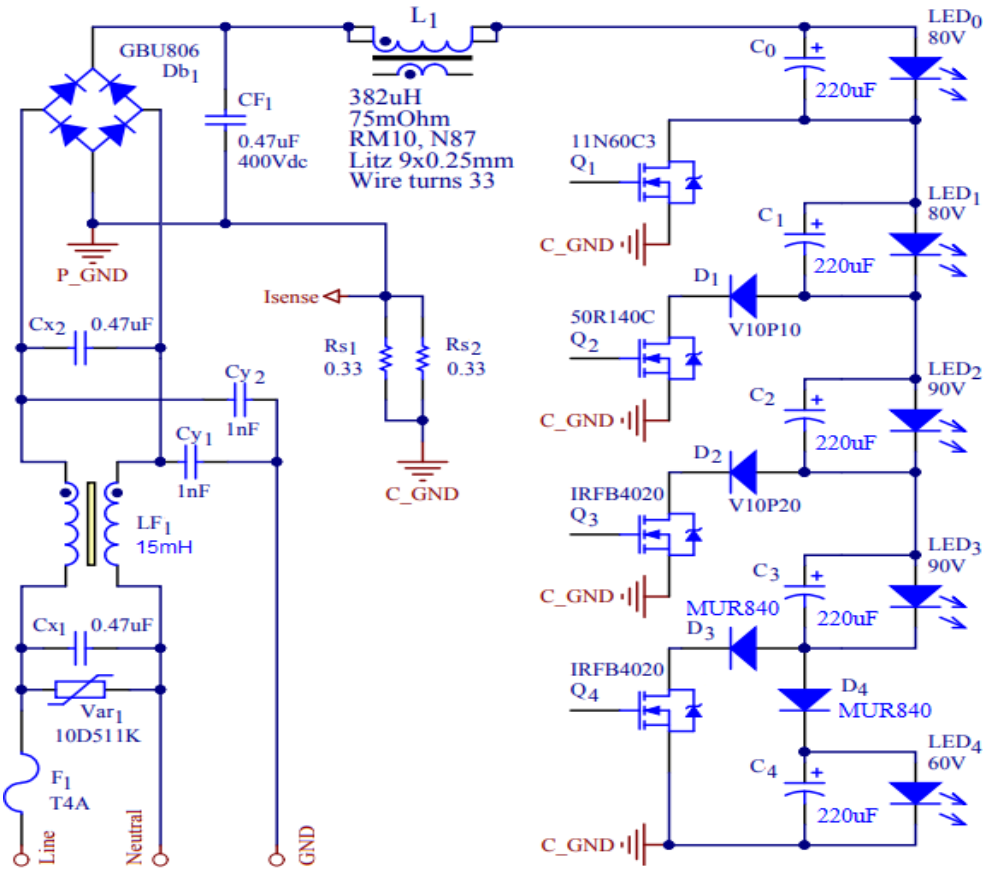

Fig. 5 The schematics of the proposed hybrid LED driver

3. Materials and Methods

3.1. Prototype Description

A first-iteration 200W laboratory prototype was developed to experimentally evaluate the operating principles of the architecture. The rated input voltage range of the prototype was 150Vac-270Vac, with an input frequency range of 43Hz-63Hz. The main power-stage circuit diagram of the prototype is shown in Figure 5. Selected electrical characteristics of the driver components are annotated directly in the circuit diagram, and a summary of the component parameters is provided in Table 1. The proposed driver has five outputs, and each output was bypassed with an electrolytic capacitor C_0-C_4 with a capacitance of 220µF, included exclusively to improve measurement accuracy by reducing voltage and current ripple in the LED string loads.

These capacitors are not necessary for the functional power-conversion topology. The boost inductor L_1 had an inductance of 382µH and was implemented using an RM10 ferrite magnetic core. The inductance of L_1 is smaller than that typically used in a conventional CCM boost driver. The hysteresis current band and inductance value were selected to maintain a switching frequency of approximately 100kHz rather than to maximize efficiency. The calculated variation of the switching frequency over a half-cycle of the mains input voltage is presented in Figure 6.

Table 1. Parameters of semiconductor components

Ref. Des.	Component	Ratings
D_1	Schottky diode V10P10	100V, 10A, V_F=0.4V (I_F=1A, T_j=25C)
D_2	Schottky diode V10P20	200V, 10A, V_F=0.52V (I_F=1A, T_j=25C)
D_3, D_4	Ultrafast diode MUR840	400V, 8A, V_F=0.9V (I_F=1A, T_j=25C)
Q_1	MOSFET SPA11N60C3	650V, 11A, R_{DS}=0.38Ω
Q_2	MOSFET IPA50R140CP	550V, 23A, R_{DS}=0.14Ω
Q_3, Q_4	MOSFET IRFB4020	200V, 18A, R_{DS}=0.08Ω
Db_1	Bridge diode GBU806	600V, 8A, V_F=0.82V (I_F=1A, T_j=25C)
L_1	Inductor, TDK core RM10	382uH, material N87, R_{DC}=75mΩ
C_0-C_4	Electrolytic capacitor, Rubycon, ZLJ series.	220uF, 120V, ESR=0.15Ω
LF_1	Common mode choke	L_{com}=15mH, L_{diff}=100µH, R=0.1Ω

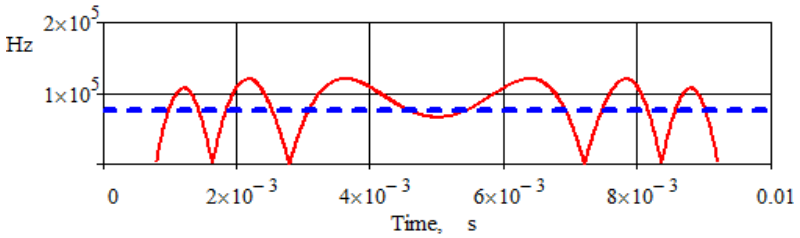

Fig. 6 Calculated instantaneous PWM frequency of the sample within half line period: blue line - the proposed driver; dotted line - 76kHz

The input-stage components, from the fuse F_1 up to the film DC capacitor CF_1 shown in Figure 5, correspond to standard practical components of a conventional CCM boost driver. The fuse F_1, varistor Var_1, filter choke LF_1, and filter capacitors Cy_1, Cy_2, Cx_1, and Cx_2 were included solely to ensure a fair comparison with a conventional state-of-the-art boost driver. Power transistors Q_1-Q_4 and protective diodes D_1-D_4 of the proposed driver were selected based on general design considerations discussed in Section 2. No exhaustive optimization of semiconductor parameters was performed at this stage.

The control circuit was realized using standard circuit solutions and operated according to the simple principles depicted in the simulation model shown in Figure 3. Input voltage and inductor L_1 current measurements were implemented using OPA607 operational amplifiers. The inductor current was measured indirectly as a voltage drop across the current-sensing resistors Rs_1 and Rs_2 (Figure 5). The upper and lower hysteresis thresholds (Comp_H and Comp_L) were implemented using two TLV3202 comparators. The resulting signals were processed by a flip-flop trigger implemented with SN74HCT00D NAND logic gates. The generated PWM signal was distributed from the flip-flop to the transistor gate drivers (MAX5048C). The transistor gate drivers were enabled or disabled by a microcontroller that realized the DEMUX block function. The selected STM32F030F4P6 microcontroller operated solely as a slow supervisory logic unit. It did not execute a control loop, generate PWM signals, perform fast timing operations, or carry out signal conditioning. Its function was limited to enabling LED strings and routing logic-level signals, operating at the mains-frequency time scale. The internal implementation of the supervisory logic does not affect the operating principle, steady-state performance, or experimental results reported in this work.

3.2. Experimental Setup and Instrumentation

The experimental setup is shown in Figure 7. The prototype was supplied from a programmable AC mains source (Chroma 61502), operated in voltage-source mode, and connected to segmented LED string loads, with high-power white LEDs connected in parallel-series and mounted on a broad aluminum printed circuit board. Natural air convection was applied to both the driver prototype and the LED load. A WT310E digital power analyzer was connected between the programmable AC source and the driver prototype to measure the input voltage, input current, power factor, and harmonic content. The WT310E has a declared measurement accuracy of 0.1%. Voltages across individual LED strings were measured using Fluke 289/FVF digital multimeters with a declared DC voltage accuracy of 0.025%. The Fluke 289/FVF multimeters were also used to measure LED string currents indirectly by recording voltage drops across high-precision RX-70 resistive current sensors with a resistance of 0.1 Ω, a tolerance of 0.01%, and a power rating of 1 W. Five current sensors were connected between the corresponding driver channels and the LED strings. All instruments operated within their specified ranges.

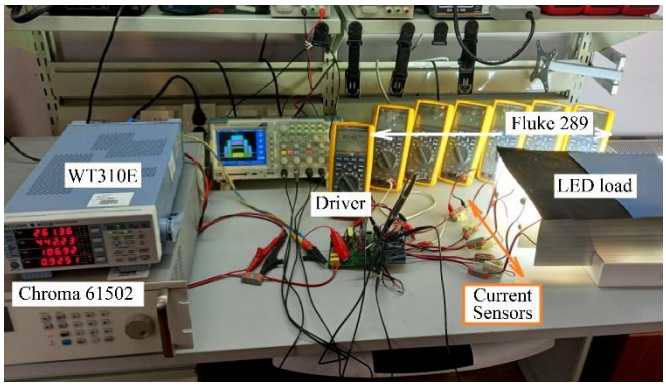

Fig. 7 The experimental set-up of the proposed driver

3.3. Experimental Measurements and Data Validation

Experimental measurements were performed using a single prototype sample at a fixed input frequency of 50Hz and input voltages of 160Vac, 230Vac, and 270Vac. For each input voltage condition, measurements were conducted over an output power range from 20W to 220W. All electrical quantities were averaged over complete mains cycles. The output voltage and current of each channel were measured using battery-powered, true-RMS Fluke 289/FVF digital multimeters. These instruments provide galvanic isolation and enable accurate measurement of DC quantities with superimposed ripple for floating differential potentials across the LED strings and current-sensing resistors. Prior to data acquisition, the system was allowed to operate for 90 min to reach steady-state thermal conditions. Steady state was confirmed by stable voltage and current readings exhibiting a drift of less than 0.1% over a 20-minute observation period. All measurement instruments were allowed to reach stable operating conditions prior to data acquisition. Identical experimental conditions, including ambient temperature and airflow, were maintained for both the prototype and the LED load throughout all tests. For each input voltage level, three independent measurement sessions were performed on separate days to account for environmental and operational variability. The reported values represent the arithmetic mean of the three measurements. The resulting standard deviation did not exceed ±0.07%, indicating high repeatability of the experimental results. Measurement uncertainty was evaluated by combining statistical uncertainty (Type A), derived from repeated measurements, and systematic uncertainty (Type B), associated with instrument accuracy. The resulting combined measurement uncertainty was below ±0.13% for all reported values.

4. Results and Discussion

4.1. Experimental Results

Figures 8 and 9 present the experimental waveforms of the transistor's drain voltage and inductor current for the proposed LED driver at 200W input power and input voltages of 160Vac, 230Vac, and 270Vac.

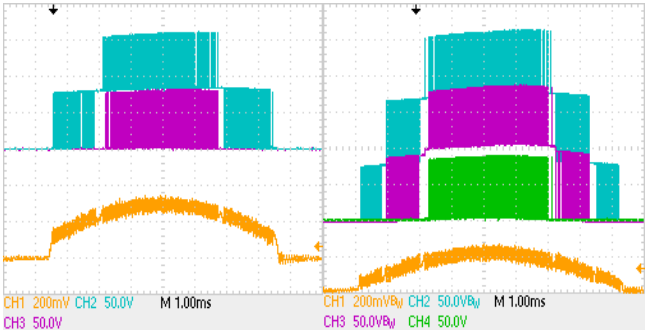

(a) **b)**

Fig. 8 Waveforms of the proposed LED driver, yellow - inductor L_1 current (current sense 0.167 Ohm), blue - voltage on the transistor Q_1, purple - voltage on the transistor Q_2, green - voltage on the transistor Q_3: (a) input 160Vac, and (b) input 230Vac.

The Waveforms of switching transistors Q_1-Q_4 and the inductor current are in good agreement with the simulated results in Figure 4, except for the switching frequency. Also, the voltage swing of transistor Q_3 is halved during Stage4 when transistor Q_4 operates in PWM mode. This deviation occurs because a V10P20 barrier capacitance of D_2 is comparable to the IRFB4020 output capacitance of Q_3, and the reverse voltage is almost equally divided between the devices. Figure 10 illustrates the transition processes between stages more clearly at *Vin*=230Vac and input power 200W. In Figure 11, the input current is compared to the inductor L_1 current.

In Table 2, harmonic measurements of the input current are presented for the proposed driver at 200W input power. Other harmonic components from the 2nd to the 40th, which are not shown in Table 2, have zero readings. The power factor is 0.98, THD is 11% at input voltage 230VAC and input power 200W.

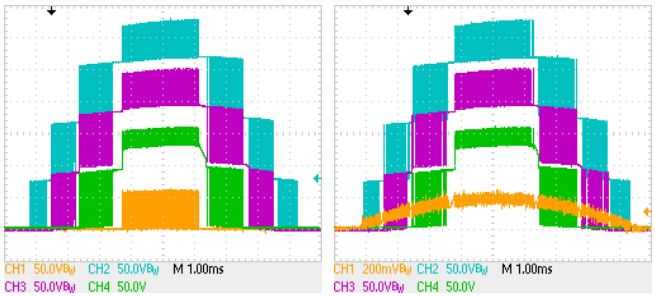

(a) (b)

Fig. 9 Waveforms of the proposed LED driver at input 270vac: (a) blue - voltage on the transistor Q_1, purple - voltage on the transistor Q_2, green - voltage on the transistor Q_3, yellow - voltage on the transistor Q_4; and (b) blue - voltage on the transistor Q_1, purple - voltage on the transistor Q_2, green - voltage on the transistor Q_3, yellow - inductor L_1 current (current sense 0.167 Ohm)

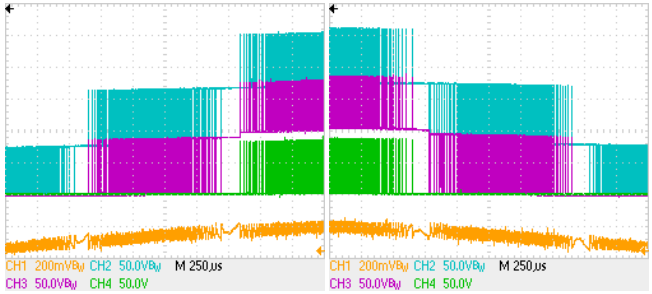

(a) (b)

Fig. 10 Experimental waveforms of the proposed LED driver, CH1- inductor L_1 curent, CH2- voltage on Q_1, CH3- voltage on Q_2, CH4- voltage on Q_3: (a) upward transitions Stage1→Stage2 →Stage3, and (b) downward transitions Stage3→Stage2→Stage1.

The power factor of the proposed driver is slightly degraded, as expected, due to the skip mode and current distortion during transitions between stages.

Finally, efficiency and power factor measurements are shown in Figure 12. At light loads, the efficiency of the proposed driver is high and exceeds that of the conventional boost LED driver. It means that the dynamic losses are smaller than expected for the proposed driver. Conduction losses prevail at high load due to two diodes operating complementarily to each other at each stage.

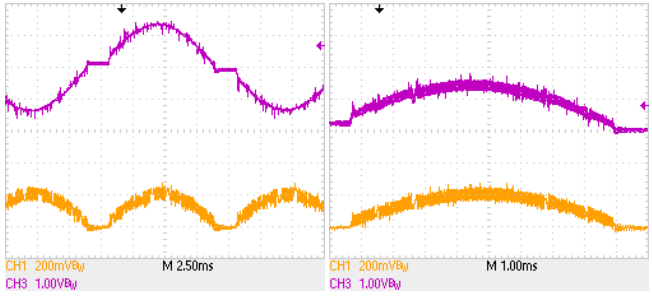

(a) (b)

Fig. 11 Input and inductor currents of the proposed driver. Red line - input current, current sense 1Ohm. Yellow line - inductor current (current sense 0.167 Ohm): (a) time resolution -2.5ms/div; and (b) time resolution -1ms/div.

Table 2. Power factor, THD (%), and Harmonics (%) measurement results

Vin	PF	THD	3	5	7	9	11	13
160Vac	0,968	9,7%	7.4	4.5	3.2	2.4	1.9	0
230Vac	0,976	10,8%	7.8	4.9	4.3	2.7	2.0	1.6
270Vac	0,968	9,8%	7.8	4.4	2.8	2.5	2.1	0

4.2. Discussion

Confirming the theoretical analysis, Figures 8 and 9 show that the amplitude of the pulsed voltages is reduced and does not exceed 90V, which is approximately five times lower than that of a conventional boost CCM driver with a 400V output.

This reduction allows for a smaller power inductor, lower magnetic losses, and decreased switching losses in the semiconductor devices. Without the inclusion of protective diodes D_1-D_4, as shown in Figure 1, stable pulsed operation of the LED strings at high power levels would not be feasible, even if electrolytic capacitors were removed from the circuit.

The inclusion of diodes D_1-D_4 is important, as they improve the reliability of the circuit. The configuration of diodes D_1-D_4 is very important for low conduction losses.

Figure 12 shows that across the load range, the efficiency of the proposed driver exceeds that of a conventional boost LED driver optimized for the 150-270Vac input range. The prototype achieved a peak efficiency of 98.6% at the nominal input of 230Vac, which is 0.3-0.4% higher than the best reported efficiencies of state-of-the-art boost-type LED drivers or boost power factor correctors [19, 20].

The efficiency increases significantly at loads below 50% and input voltages ranging from 160Vac to 270Vac. This indicates reduced switching losses, as theoretically expected. As the load increases, diode conduction losses become dominant, evidenced by nearly a linear decrease in efficiency.

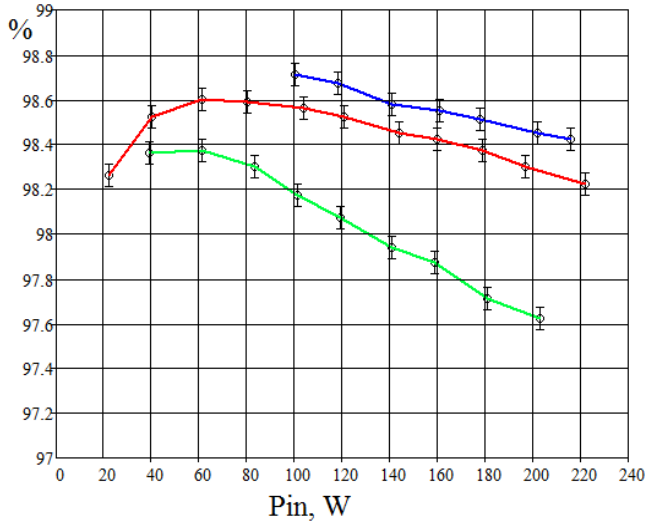

(a)

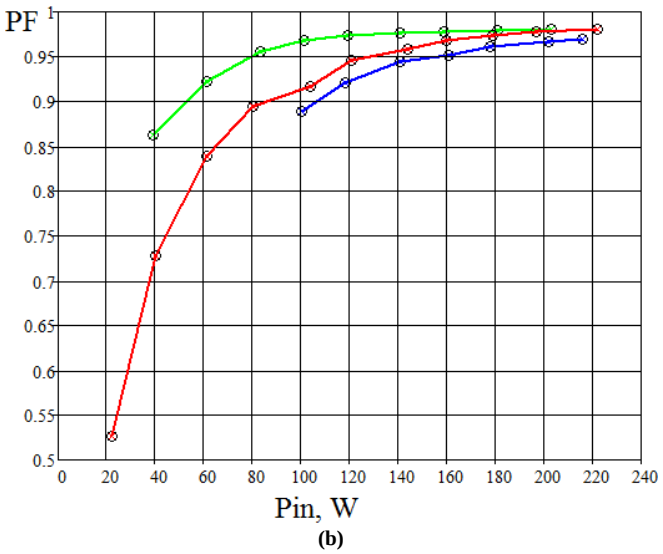

(b)

Fig. 12 Efficiency and power factor measurements of the driver, blue - at 270Vac input, red - at 230Vac input, green - at 160Vac: (a) Efficiency, and (b) Power factor.

At 160Vac, only two stages operate during the input phase cycle - only transistors Q_1 and Q_2 are active (as shown in Figure 8(a)), along with Schottky diodes D_1 and D_2. At 230Vac, three stages operate (as shown in Figure 8(b)), activating transistors Q_1-Q_3 and diodes D_1-D_3. At 270Vac, all stages operate sequentially, involving transistors Q_1-Q_4 and diodes D_1-D_4 (as shown in Figure 9).

However, in any active stage, only two diodes are involved, operating complementarily such that only one conducts at a time. The lower the input voltage, the fewer LED strings receive the full output power of the developed prototype. Therefore, the nominal input voltage must not fall below 150Vac in order to prevent overloading of the lower-indexed LED strings. But the lower limits of the input voltage range can be expanded with appropriate derating of the nominal power.

The LED_0 string helps to introduce skip mode. Skip mode moderately degrades the power factor, but reduces switching losses at low input voltages. The presence of the LED_0 string reduces component stress at high input voltages. Here, a trade-off exists between expanding the skip-mode range, semiconductor voltage stress, and efficiency on the one hand, and power factor degradation on the other. Current distortions during transitions between stages, see Figure 11, also add to the PF worsening. However, PF is not dramatically impacted by these factors. As shown in Table 2, harmonics are within the key IEC61000-3-2 Class C requirements.

Table 3 presents a comparison of the proposed LED driver with the conventional drivers based on existing technologies. Table 4 summarizes the component loss breakdown of the proposed hybrid driver at 230Vac and rated power. From Table 3, it can be observed that conventional boost PFC drivers offer high efficiency and scalability but suffer from large inductors and high-voltage stress on components, making them unsuitable for compact, high-power integration. Direct AC LED modules, while structurally simple, exhibit high conduction losses due to linear current regulation, therefore limited scalability. Conventional hybrid LED drivers, which combine switching and reconfiguration techniques of the LED load, fall between boost converters and direct AC modules in terms of complexity. However, they still experience hard switching and significant EMI issues at higher power levels.

The proposed improved hybrid driver has significantly reduced switching stresses on power components, which opens the way to high-voltage and high-power applications. Because of its modular structure, the driver can be readily scaled to various power levels (50-300W) and input voltages by adjusting the number of LED strings and switching devices, which is advantageous for both indoor and outdoor lighting applications such as street lamps, industrial fixtures, and commercial luminaires.

The current design supports operation at input voltages up to 275Vac, covering international grid standards, and maintains high efficiency and power factor across this range. Its robust control strategy enables reliable performance under variable line and load conditions, making it well-suited for retrofit or integrated lighting applications where reliability and lifetime are critical. The design could operate without electrolytic capacitors and bulky inductors as well, enabling a smaller form factor and lower manufacturing costs.

Since the protective diodes are connected in such a way that only one diode conducts at any given time, further segmentation of the LED load into smaller strings does not increase conduction losses in the diodes. However, it reduces switching losses in the semiconductors and in the power inductor. Therefore, increasing the circuit complexity through additional LED segmentation can actually enhance the overall efficiency of the proposed driver.

Owing to the low losses in the power semiconductors, the proposed architecture is compatible with monolithic integration of the control circuit and power transistors, paving the way for low-cost System-on-Chip (SoC) LED driver solutions. This integration could substantially improve production yield, reliability, and lifecycle performance compared to discrete designs. From Table 4, the 1.4W loss in the bridge rectifier exceeds the combined 1.3W loss in the inductor and the remaining semiconductors. Of that 1.3W, only about half ≈0.7W, corresponds to switching losses, if components are properly optimized. Consequently, for a driver that employs a diode bridge, further segmentation of the LED load (i.e., increasing the number of LED strings) is unlikely to deliver a meaningful efficiency gain and would mainly add circuit complexity.

Table 3. Comparison with existing driver technologies

Technology	PWM	Power	Input Voltage	Eff.	THD	PF	Strings	Inductor value/size	Input filters	Integration
CrCM Boost PFC [19]	>40kHz	300W	230Vac	<98.2%	12.3%	0,97	1	250uH, PQ3230	Two	No
CCM Boost PFC [20]	100kHz	1200W	230Vac	<98.2%		0,998	1	680uH	One	No
AC direct module [9]	No	10W	100Vac	85%	3.2%	0.999	4	No	No	No
AC direct module [13]	No	15W	<140Vac	84.7%		0.973	3	No	No	No
AC direct module [14]	No	12W	110Vac	88.2%		0.905	8	No	No	Yes
Hybrid [18]	<5MHz	17W	240Vac	<94%		0.923	7	47uH		Yes
Hybrid [17]	<5MHz	20W	110Vac	<95.1%		0.986	7	6.8uH	One	Yes
This Work	<120kHz	200W	230Vac	<98.6%	11%	0.976	5	382uH, RM10	One	Not yet, but possible

Table 4. Component power losses at Vin = 230Vac, Pin = 200W, η = 98.3%

	Total of Hybrid driver	Bridge diode, Db_1	Input filter, LF_1	Control	PCB	Inductor, L_1	Capacitors, C_0-C_4	Semiconductors, Q_1-Q_4 and D_1-D_2
Power loss	3.4W	1.4W	0.2W	0.1W	0.1W	0.4W	0.3W	0.9W

By contrast, for a monolithically integrated solution that incorporates both control and power switches, additional segmentation becomes attractive, as it reduces on-chip losses, die heating, and the amplitude of pulsed voltages.

The prototype hybrid driver requires optimization with respect to inductor size, hysteresis current band, switching frequency, and overall efficiency. In addition, the semiconductor components require balancing the trade-off between switching and conduction losses.

5. Conclusion

This work presented an improved hybrid LED driver topology designed for high-power and high-voltage lighting applications. Unlike conventional hybrid LED drivers, the proposed design employs protective diodes connected in series with MOSFETs, effectively reducing switching stress without introducing significant conduction losses.

The driver was theoretically analyzed, and a first iteration 200W laboratory prototype with five LED strings was developed and tested under input voltages of 160-270Vac. Experimental verification demonstrated a high efficiency of 98.6% at 230Vac, with a power factor of 0.98 and THD of 11%, in good agreement with theoretical predictions.

The driver's performance was compared against existing LED driver technologies, showing superior efficiency and reduced component stress. The inclusion of protective diodes ensures reliable operation by preventing reverse current flow while maintaining low conduction losses and enabling segmentation of the LED load in a manner that reduces switching losses rather than increasing conduction losses, in contrast to conventional hybrid driver topologies.

This fundamentally alters the trade-off between efficiency, component stress, and scalability in high-power LED systems. Owing to its low switching losses and simple control principles, the proposed driver is well suited for both discrete implementations and future monolithic integration of control and power stages. Such integration has the potential further to reduce losses, component count, and system size, while improving reliability and manufacturability.

Additionally, proposed skip-mode operation and optimized power semiconductor selection enable a favorable trade-off between efficiency, component stress, and power quality while maintaining compliance with IEC61000-3-2 Class C requirements. Future work will focus on determining the optimal number of LED strings, further optimizing power-stage parameters, and developing a control strategy to enhance efficiency and power quality over a wider operating range.

Scaling of the proposed architecture to different power levels and LED configurations will also be considered to broaden its applicability.

Funding Statement

This work was funded by the Science Committee of the Ministry of Education and Science of the Republic of Kazakhstan under project AP No.19678370, titled "Research and Development of a hybrid LED driver".

References

[1] Osram, Reliability and Lifetime of LEDs Appication Note, 2013. [Online]. Available: https://www.osram.com/Graphics/XPic6/00102625_0.pdf

[2] Hui Zhang, "Reliability and Lifetime Prediction of LED Drivers," *2017 14th China International Forum on Solid State Lighting: International Forum on Wide Bandgap Semiconductors China (SSLChina: IFWS)*, Beijing, China, pp. 24-27, 2017. [CrossRef] [Google Scholar] [Publisher Link]

[3] Xiaohui Qu et al., "A Lifetime Prediction Method for LEDs Considering Real Mission Profiles," *IEEE Transactions on Power Electronics*, vol. 32, no. 11, pp. 8718-8727, 2016. [CrossRef] [Google Scholar] [Publisher Link]

[4] Murat Demir, Ali Bekir Yildiz, and Tayfun Ağir, "Observation of the Effects of Electrostatic Discharge and Lightning Surge on the Reliability of a LED Circuit Driven by Half-Bridge Converter," *2018 International Symposium on Power Electronics, Electrical Drives, Automation and Motion* (*SPEEDAM*), Amalfi, Italy, pp. 1073-1078, 2018. [CrossRef] [Google Scholar] [Publisher Link]

[5] P. Watté et al., "Reliability of Electronic Drivers: An Industrial Approach," *2021 18th China International Forum on Solid State Lighting & 2021 7th International Forum on Wide Bandgap Semiconductors* (*SSLChina: IFWS*), Shenzhen, China, pp. 246-249, 2021. [CrossRef] [Google Scholar] [Publisher Link]

[6] A.P. Sachintha, and G. De Vas Gunawardena et al., "LED Driver Useful Life: New Research on Multiple Component Degradation and Their Effects on Driver Life," *Lighting Design+ Application*, vol. 53, no. 5, pp. 56-58, 2023. [CrossRef] [Google Scholar] [Publisher Link]

[7] H. Niu et al., "Lifetime Prediction of Aluminum Electrolytic Capacitors in LED Drivers Considering Parameter Shifts," *Microelectronics Reliability*, vol. 88-90, pp. 453-457, 2018. [CrossRef] [Google Scholar] [Publisher Link]

[8] Bo Liu et al., "Consistency and Degradation of Electrochemical Double Layer Capacitors under Calendar Ageing," *2020 Global Reliability and Prognostics and Health Management* (*PHM-Shanghai*), Shanghai, China, pp. 1-5, 2020. [CrossRef] [Google Scholar] [Publisher Link]

[9] K.I. Hwu, and W.C. Tu, "Controllable and Dimmable AC LED Driver Based on FPGA to Achieve High PF and Low THD," *IEEE Transactions on Industrial Informatics*, vol. 9, no. 3, pp. 1330-1342, 2013. [CrossRef] [Google Scholar] [Publisher Link]

[10] Yutsung Yeh et al., "AC Direct Multiple-String LED Driver with Low THD and Minimum Components," *2015 International SoC Design Conference (ISOCC)*, Gyeongju, Korea (South), pp. 117-118, 2015. [CrossRef] [Google Scholar] [Publisher Link]

[11] Hongbo Gao et al., "An Electrolytic-Capacitorless and Inductorless AC Direct LED Driver with Power Compensation," *2015 IEEE 2nd International Future Energy Electronics Conference* (*IFEEC*), Taipei, pp. 1-5, 2015. [CrossRef] [Google Scholar] [Publisher Link]

[12] Hui Zhang, "Developing Highly Reliable LED Luminaries for High Temperature Applications using AC-Direct Driving LED Technology," *2018 IEEE Applied Power Electronics Conference and Exposition* (*APEC*), San Antonio, TX, USA, pp. 3466- 3470, 2018. [CrossRef] [Google Scholar] [Publisher Link]

[13] Yuichi Noge, "Experimental Verification of a Linear AC LED Driver with a Light Flicker Compensating Circuit and High Power Factor Operation by Modulating the Current Regulator," *IEEJ Transactions on Industry Applications*, vol. 139, no. 9, pp. 814-821, 2019. [CrossRef] [Google Scholar] [Publisher Link]

[14] Seong Jin Yun, Yong Ki Yun, and Yong Sin Kim, "A Low Flicker TRIAC Dimmable Direct AC LED Driver for Always-on LED Arrays," *IEEE Access*, vol. 8, pp. 198925-198934, 2020. [CrossRef] [Google Scholar] [Publisher Link]

[15] San-Fu Wang et al., "Ultra-Low Percentage Flicker High-Efficiency Direct AC LED Driver using Constant Power Technology," *IEEE Access*, vol. 11, pp. 97400-97407, 2023. [CrossRef] [Google Scholar] [Publisher Link]

[16] Hsiao-Hsing Chou, "Design and Implementation of the Linear LED Driver," *IEEE Transactions on Circuits and Systems II: Express Briefs*, vol. 70, no. 3, pp. 1059-1063, 2023. [CrossRef] [Google Scholar] [Publisher Link]

[17] Lisong Li, Yuan Gao, and Philip K.T. Mok, "A Multiple-String Hybrid LED Driver with 97% Power Efficiency and 0.996 Power Factor," *2016 IEEE Symposium on VLSI Technology*, Honolulu, HI, USA, pp. 1-2, 2016. [CrossRef] [Google Scholar] [Publisher Link]

[18] Yuan Gao et al., "A Hybrid LED Driver With Improved Efficiency," *IEEE Journal of Solid-State Circuits*, vol. 55, no. 8, pp. 2129-2139, 2020. [CrossRef] [Google Scholar] [Publisher Link]

[19] Kwun-Hok Chong, Yuan Gao, and Philip K.T. Mok, "A Customized AC Hybrid LED Driver With Flicker Reduction for High Nominal Range Applications," *IEEE Transactions on Circuits and Systems II: Express Briefs*, vol. 68, no. 5, pp. 1635-1639, 2021. [CrossRef] [Google Scholar] [Publisher Link]

[20] ON Semiconductor, Power Factor Correction (PFC) Handbook, Application Note HBD853/D, 2014. [Online]. Available: https://www.onsemi.com/pub/collateral/hbd853-d.pdf

[21] Sam Abdel-Rahman, Franz Stückler, and Ken Siu, "PFC Boost Converter Design Guide," *Infineon Application Note*, 2016. [Google Scholar]